



# CHORUS

This is the accepted manuscript made available via CHORUS. The article has been published as:

## Metal-induced charge transfer, structural distortion, and orbital order in SrTiO<sub>3</sub> thin films

Jaekwang Lee, Chungwei Lin, and Alexander A. Demkov

Phys. Rev. B **87**, 165103 — Published 3 April 2013

DOI: [10.1103/PhysRevB.87.165103](https://doi.org/10.1103/PhysRevB.87.165103)

# Metal-induced charge transfer, structural distortion and orbital order in SrTiO<sub>3</sub> thin films

Jaekwang Lee<sup>1</sup>, Chungwei Lin and Alexander A. Demkov<sup>2</sup>

Department of Physics, The University of Texas at Austin, Austin, TX 78712, USA

## Abstract:

The atomic and electronic properties of the Cs/SrTiO<sub>3</sub> heterostructure are investigated using density-functional theory (DFT). Our results suggest that an antiferrodistortive (AFD) or a ferroelectric (FE)-like distortions could be induced in SrTiO<sub>3</sub> (STO) by a Cs layer, depending on the interface bonding geometry between the metal and the oxide. Furthermore, while the AFD distortion extends throughout the STO region, the FE-like distortion decays within two layers of STO. Independent of the interface geometry, we find a large  $e_g$  orbital splitting (orbital order) around the interface, leading to an  $e_g$ -based two-dimensional electron gas (2DEG) confined within the two layers of STO, which is fundamentally different from the conventional  $t_{2g}$ -based 2DEG in this material. This unique feature can be understood in terms of the local orbital mixing at the interface. We discuss the relation between the orbital order and structural distortion.

## 1. Introduction

SrTiO<sub>3</sub> (STO) is a prototypical perovskite that does not possess many of the functional properties of the other members of this group of materials. The Ti  $3d$   $t_{2g}^*$  band is

---

<sup>1</sup> Present address: Oak Ridge National Laboratory

<sup>2</sup> E-mail: demkov@physics.utexas.edu

empty, rendering STO nonmagnetic. Instead of the FE transition observed in BaTiO<sub>3</sub>, STO is known to undergo an AFD transition, corresponding to out-of-phase rotations in neighboring planes of TiO<sub>6</sub> octahedra, but only when the temperature drops below 110 K [1-5]. Despite these “shortcomings”, STO is a very interesting material in its own right. In particular, a recent discovery by Hwang and co-workers of the two dimensional electron gas (2DEG) at the interface of STO and LaAlO<sub>3</sub> (LAO) [6] has sparked a revival in STO research [6-13]. The origin of the 2DEG is still controversial [7,8]. We have recently suggested that at the STO/LAO interface, the initial crystal field-induced splitting of the Ti- $t_{2g}^*$  band is increased dramatically to 0.4 eV once the charge is transferred into STO through the electrostatic doping [13]. We have argued that this charge transfer results in the Jahn-Teller (JT) distortion and charge localization that is ultimately responsible for the formation of the 2DEG at the interface. It is worth noting that the state responsible for this 2DEG is a  $d_{xy}$  orbital of the  $t_{2g}^*$  band.

To further explore the effects of charging the STO  $t_{2g}^*$  band, we consider theoretically heterostructures comprised of STO and Cs, a metal with a very low work function ( $\sim 2.2$  eV) [14-16]. Because of its small work function, the adsorption of Cs on various materials, such as Si, GaAs and GaN has been widely studied [17-23]. The electron affinity of STO is approximately 4.0 eV, so the Fermi level of Cs falls well into the conduction band of STO, at least within the Schottky picture. Therefore, we can expect charge transfer into the conduction band of STO to be rather significant and sufficient to trigger interesting and unusual effects.

Using density functional theory, we find that both the FE-like and AFD distortions can be induced in STO by Cs, depending on the details of the interfacial bonding geometry between the two materials. Moreover, we find that the AFD distortion extends throughout

the entire STO region (nine layers of STO symmetrically terminated with TiO<sub>2</sub>), whereas the FE-like distortion survives only up to the second layer of STO. We also find that, independent of the interface geometry, a large  $e_g$  orbital splitting, or orbital order, occurs near the interface, with the  $3d_{z^2}$  level shifting 2.0 eV below  $3d_{x^2-y^2}$ . This ultimately leads to an  $e_g$ -based 2DEG confined within two layers of STO near the interface. This feature is quite unique since typically the 2DEG at the interface is derived from the  $t_{2g}$  orbitals [12,13] because in bulk STO they have lower energy than the  $e_g$  bands due to a large crystal field effect.

The rest of the paper is organized as follows. After briefly describing the computational details we analyze the band alignment and charge transfer at the Cs/STO interface. We then describe two structural distortions induced by the metal, and discuss the orbital character of the 2DEG forming at the interface.

## 2. Computational details

We use density functional theory within the local spin density approximation (LSDA) as implemented in the Vienna *Ab initio* Simulation Package (VASP) code [24, 25] and projector augmented wave (PAW) pseudopotentials. We use a kinetic energy cut off of 600 eV, and 8x8x8 (bulk) and 8x8x1 (slab) k-point meshes for the Brillouin zone integration. The calculations are converged in energy to  $10^{-6}$  eV/cell, and the structures are relaxed until the forces are less than  $2 \times 10^{-2}$  eV/Å. To model the epitaxial Cs/STO structure, we use a mirror symmetric cell that includes two (STO)<sub>9</sub>(Cs)<sub>7</sub> slabs separated by 16 Å of vacuum, with two identical interfaces as shown in Fig. 1. Here the subscript refers to the number of total SrO and TiO<sub>2</sub> layers and to that of Cs layers. The STO region is

symmetrically terminated with the TiO<sub>2</sub> layer. Since our geometry has complete mirror symmetry with respect to vacuum in the middle region, the local potential profile satisfies the periodic condition at the boundary, even if there is a field across each slab. Thus, we can correctly analyze the profile of the local potential across the STO layer without a dipole correction. For bcc Cs, we find the lattice constant to be 5.65 Å using the LSDA, compared to the experimental value of 6.05 Å [26-28]. In order to match the experimental band gap of STO, we apply a Hubbard U correction using a rotational invariant scheme [29]. Using U<sub>3d</sub> = 8.5 eV we obtain E<sub>g</sub>=3.2 eV and lattice constant of 3.94 Å. Both are in good agreement with the experimental values of E<sub>g</sub>=3.2 eV and 3.91 Å, respectively. Even though the U is rather large, this value correctly reproduces the  $t_{2g}^*$  orbital ordering at the STO conduction band bottom and the crystal field splitting. Both are in agreement with the photoemission data and have been checked with the hybrid functional calculation [30,31]. In order to consider an epitaxial film of Cs on the STO substrate, the in-plane lattice constant of the slab is fixed to  $\sqrt{2} a_{\text{STO}}=5.576$  Å (rotated by 45° with respect to the cubic unit cell) as shown Fig. 1. Cs metal is therefore under biaxial compressive strain of -1.3 % due to the lattice mismatch. To accommodate strain induced in the Cs layer, we optimize the out of plane lattice constant of Cs. We obtain 6.1 Å through the total energy minimization. The lattice constant of Cs within GGA is 6.13 Å, which is only 1.3% off compared to the experimental value. Here we use the LDA value for Cs for overall consistency. We are considering an epitaxial film of Cs on the STO substrate, and the lattice constant of STO within the LDA+U (3.94 Å) is in much better agreement with experimental value of 3.905 Å than that within the GGA+U (4.03 Å).

We investigate two different arrangements of Cs on the TiO<sub>2</sub> terminated surface of STO. First, Cs atoms are positioned atop the “hollow sites” surrounded by four in-plane oxygen atoms as shown in Fig. 1 (a). This structure will be referred to as a “hollow site interface”. Second, Cs atoms are positioned directly above the “oxygen sites” as shown in

Fig. 1 (b). In what follows, we will call this an “oxygen site interface”. In both arrangements there is one Cs atom per surface unit cell, which corresponds to half mono layer coverage of the STO substrate. These two different arrangements contain the same number of atoms (the total number of atom is 106). As will be discussed later, the relaxation has a similar effect on the electronic structure of STO for two interface geometries but a totally different effect on the atomic distortion of STO.

### 3. Results

#### 3.1 Schottky Barrier at the Cs/STO Interface.

In order to explore the charge transfer from Cs to the conduction band of STO, we first need to determine the work function (WF) of Cs ( $\phi_M$ ), and the ionization potential ( $I_s$ ) and electron affinity ( $\chi_s$ ) of STO. Using the averaged potential method with the isolated, symmetrically terminated Cs slab at the local spin density approximation level (LSDA), the WF is calculated as the difference between the Fermi energy of the slab and the value of the electrostatic potential in the vacuum region. We find 2.2 eV in good agreement with the experimental value of 2.14 eV. The ionization potential ( $I_s$ ) of STO is defined as the energy difference between the valence-band maximum and the vacuum level. Using a symmetric, TiO<sub>2</sub>-terminated STO slab we find the value of 5.65 eV at the LSDA+U level. Since the band gap of STO is 3.2 eV at the LSDA+U level, the electron affinity can be also estimated as 2.45 eV. Thus, the Fermi level of Cs is expected to be 0.25 eV higher than the STO conduction band bottom as shown in Fig. 2(a). And we expect that electrons would transfer from Cs to the conduction band of STO.

The TiO<sub>2</sub>-terminated STO surface exhibits a surface oxygen state at the top of the valence band. This state is composed of the lone-pair oxygen  $2p$  orbitals oriented normal to the Ti-O-Ti bonds in the surface plane. These surface states place the highest occupied STO

level 0.9 eV ( $\Delta_s$ ) higher than the bulk valence band top as indicated in Fig. 2(a), and can be thought of as the charge neutrality level (CNL) [32, 33].

After bringing the Cs metal and TiO<sub>2</sub> terminated STO slab in contact, the value of  $\Delta_s$  is still 0.9 eV (see Fig. 4 (a)), suggesting that  $\Delta_s$  is not affected by the presence of the metal. The Fermi level of Cs is approximately 1.3 eV lower than the STO conduction band bottom (see Fig. 4 (a)). This value directly corresponds to the n-type Schottky Barrier (SB) indicated in Fig 2. (b) as  $\phi_n$ . According to the metal induced gap states theory [34, 35], the n-type SB is expressed as

$$\phi_n = S(\phi_M - \chi_S) + (1-S)\phi_{CNL} \quad (1)$$

where  $S$  is a dimensionless pinning parameter that depends on the density and extent of the interfacial states in the insulator [36, 37], and  $\phi_{CNL} = 2.3eV$  is the CNL determined with respect to the bottom of the conduction band of STO as indicated in Fig. 2(b). Demkov *et al.* [38] have previously reported the CNL of 2.0 eV in fair agreement with our calculated value of 2.3 eV.

Using 1.3 eV for the n-type SB height in Eq. 1, we obtain  $S=0.4$ . Reported experimental values of  $S$  vary between 0.1 and 0.6 [39-41]. The pinning factor  $S$  can be also estimated using an empirical formula [42]:

$$S = \frac{1}{1 + 0.1(\epsilon_\infty - 1)^2} \quad (2)$$

where,  $\epsilon_\infty$  is the electronic dielectric constant of STO. Using the experimentally measured value of  $\epsilon_\infty = 5.2$  for STO [43], we obtain  $S = 0.36$  in good agreement with our result. The values of SB and S are the same for both interface structures (hollow and oxygen site interfaces), suggesting that the relaxation has a similar effect on the electronic structure of STO for both geometries.

### 3.2 Dependence of atomic reconstruction on interface geometry.

We now explore atomic distortions of STO for two Cs/STO interfaces with the hollow site geometry. The FE-like lattice distortion occurs as depicted in Fig. 3 (a). To quantify the FE-like distortion, the relative displacement of Ti with respect to the oxygen atom (the so-called rumpling) is calculated. The rumpling is about 0.1 Å at the 1<sup>st</sup> TiO<sub>2</sub> layer (interfacial layer with Cs) and then abruptly drops to zero at the 3<sup>rd</sup> layer. Negative rumpling occurs at the surface TiO<sub>2</sub> layer, indicating that Ti moves away from vacuum. Such an atomic distortion is consistent with what happens at the TiO<sub>2</sub>-terminated STO surface. Thus, negative rumpling is closely related to the surface reconstruction of STO. In contrast, positive rumpling (FE-like lattice distortion) is expected to be attributed to charge transfer from the Cs metal into STO. We will discuss this effect in more detail in the next section.

In the oxygen site interface geometry, instead of the FE-like lattice distortion, opposite rotations of TiO<sub>6</sub> octahedra in adjacent cells (corresponding to bulk AFD distortion) happen as shown in Fig. 3 (b). The ratio of the lattice parameters  $c/a$  is 1.002 due to the tetragonal phase transformation, which is in good agreement with the experimental value of 1.0006 [44]. However, the oxygen octahedron rotation angle is 7 degrees for the interfacial Ti and 10 degrees for Ti in the middle region. These values are larger than those obtained for bulk STO in experiment (2.1 degree) and theory (5.5 degree [45]). We suggest that such a large octahedral rotation is induced by Cs-O bonding at the Cs/STO interface. For the hollow site interface, four oxygen atoms are equivalent, and their positions are

invariant under the  $C_4$  operation [46]. In comparison, at the oxygen site interface three oxygen ( $O_C$ ,  $O_F$ ,  $O_M$ ) atoms are not equivalent. The  $O_C$  atom right below Cs shifts towards Cs as indicated in Fig. 3 (b). However, atomic positions of  $O_F$  and  $O_M$  are almost unchanged. As a result, an AFD distortion develops. In other words, the inequivalent atomic positions of oxygen with respect to Cs lead to the different atomic displacements, resulting in AFD distortion. At the LSDA+U level, two structures are almost degenerate (FE is  $\Delta=0.03$  eV per simulation cell lower in energy) and at the LSDA level they are very close in energy with FE structure still being a ground state ( $\Delta=1.43$  eV per simulation cell).

### 3.3 Charge transfer at the Cs/STO interface

In order to compare the extent of the atomic distortion and that of the transferred charge, we plot the density of states projected on the interfacial layer of Cs and 9 layers of STO (PDOS) for two interfacial geometries in Fig. 4 (a). We assume that bulk  $\text{TiO}_2$  layer is the 3<sup>rd</sup> one below the 1<sup>st</sup> layer of Cs as the bulk electronic structure is recovered (thick red arrow). The surface oxygen state is 0.9 eV ( $\Delta_s$ ) higher than the bulk valence band top. From the PDOS, we can clearly see significant charge transfer up to the second  $\text{TiO}_2$  layer for both interface geometries. This spatial extension is similar to that of FE-like distortion induced at the hollow site interface. Thus, we suggest the FE-like distortion of STO is directly driven by charge transfer from Cs metal. In contrast, the AFD distortion extends throughout the entire STO film (Fig. 3(b)) but charge is transferred only through the second  $\text{TiO}_2$  layer. Thus, we point out that the AFD distortion is not directly caused by the charge transfer. Instead of the charging, the inequivalent atomic positions of oxygen with respect to Cs lead to the different atomic displacements, resulting in the AFD distortion. We integrate the PDOS within an energy window of 0.5 eV below the Fermi energy ( $E_F$ ) up to  $E_F$  to show how charge is distributed through the STO layer along the stacking direction. In Fig. 4 (a), the partially occupied Ti-d states are evidently created by the charge transfer from the Cs metal, as STO is an insulator with no states in the middle of the gap. The

amount of charge transfer can be directly computed by integrating the partially occupied Ti- $d$  states. The result in the units of  $e/\text{\AA}$  is plotted in Fig. 4 (b). The vertical line corresponds to the position of the interfacial  $\text{TiO}_2$  layer after full atomic relaxation. The transferred charge distribution is fitted with the exponential function. The evanescent state decay lengths  $\beta$ , corresponding to the slope in the log plot, are 1.7 and 1.8  $\text{\AA}$  for the FE-like and AFD distorted structures, respectively. The numbers are similar because  $\beta$  is known to be intrinsic to the insulator. Our values are in agreement with that obtained from the complex band structure calculation for the STO [38]. The total transferred charge is 0.3e for the FE-like and 0.25e for the AFD distorted structures, respectively. These values are approximately ten times larger than that reported for the STO/LAO heterostructure. In the STO/LAO heterostructure, the charge transfer happens through electrostatic doping. Thus, direct charge transfer from a metal reservoir is a more effective way to generate a 2DEG.

### 3.4 Orbital order and transferred charge distribution.

In contrast to the STO/LAO interface [13], a strong  $e_g$  orbital order, with  $d_{z^2}$  orbital 2.0 eV lower than  $d_{x^2-y^2}$ , occurs near the Cs/STO interface. This can be understood as follows. Locally, the Ti atom at the Cs/STO interface is under the square pyramidal symmetry that splits  $t_{2g}$  into  $d_{xy}$ , and  $d_{xz} + d_{yz}$  and  $e_g$  into  $d_{x^2-y^2}$  and  $d_{z^2}$ , respectively. Recently, Lin *et. al.* have pointed out that for a transition metal perovskite under a symmetry-reduced environment (cubic to  $C_{4v}$ ), such as in the presence of a vacancy or an interface, a complete picture of the level splitting should include the  $4s$  and  $4p$  components [31]. In particular, the hybridization between  $3d_{z^2}$  and  $4p_z$  orbitals can be strong, which pushes the  $3d_{z^2}$  level down significantly, as illustrated in Fig. 5 (a). Indeed, by plotting the orbital decomposed DOS of Ti next to the interface in Fig 5 (b), we see that the Ti  $4p_z$

strongly hybridizes with  $3d_{z^2}$  orbital since their peak positions coincide. To visualize the orbital order, we show the isosurface plot of transferred charge for the Cs/STO slab with the AFD and FE-like distortions in Figs. 6 (a) and (b), respectively. We can clearly see the  $d_{z^2}$  orbital order from the dumbbell-like charge distribution along the STO stacking direction.

As can be seen from our calculations, *both* charge transfer and  $e_g$  orbital order happen only within the first two layers of STO, suggesting these two phenomena are related. At the LAO/STO interface, the local symmetry at the Ti site is still very close to cubic; therefore the lowest conduction band state is  $t_{2g}$ -based. The charge transfer causes local distortion, splitting the  $d_{xy}$  orbital and localizing the charge [13]. In the present case, however, the symmetry is strongly reduced from cubic, causing the local mixing of  $3d$  and  $4p$  orbitals. This enables a  $3d_{z^2}$ -based interfacial state rapidly decaying into the bulk to develop. It is worth noting that such a state has a large overlap with the metal layer, facilitating the charge transfer. Deeper into STO the conduction band bottom recovers its  $t_{2g}$  character (not shown). Charging these states might have induced a JT-like distortion similar to LAO/STO case. However, as charge is captured by  $e_g$ -based interfacial states, this does not happen, and rumpling caused by charging one of the  $e_g$  states rapidly decays. The system's response thus appears to be localizing charge in  $e_g$  states that can be easily pushed down owing to strong hybridization with  $p_z$  orbitals.

## 4 CONCLUSIONS

Using density functional theory, we study the STO/Cs interface and find that, depending on the details of the interfacial bonding geometry between STO and Cs, both FE-like and AFD distortions can be induced in STO by the metallic overlayer. The AFD distortion extends through the entire STO region, whereas the FE-like distortion survives only through the second layer of STO. We find a large charge transfer of  $0.2e$  from Cs into STO. This is approximately ten times larger than that reported for the STO/LAO heterostructure, suggesting that direct charge transfer from a low work function metal is more effective than that through electrostatic doping. Interestingly, we find that regardless of the induced structural distortion, charge transfer is largely complete within two layers of STO. The spatial extension of the FE-like distortion is identical to that of charge transfer, indicating the FE-like distortion is directly induced by the charge transfer. A strong  $e_g$  splitting (orbital order) happens near the interface, which is justified and visualized through the isosurface plot of transferred charge distribution. We show that the energy lowering of the  $3d_{z^2}$  orbital ( $e_g$  orbital order) is accompanied by a strong hybridization with the  $4p_z$  orbital, making the state more extended and easier to hybridize with orbitals of nearby atoms. The resulting  $3d_{z^2}-4p_z$  evanescent states are occupied by the transferred electrons, leading to a unique  $e_g$ -based 2DEG at the STO side of the interface.

## ACKNOWLEDGEMENTS

This work is supported by the National Science Foundation under grant DMR-0548182, and the US Department of Energy under grant DE-SC0001878. All calculations are done at the Texas Advanced Computing Center.

## REFERENCES

1. E. Heifets, E. Kotomin and V. A. Trepakov, *J. Phys. :Cond. Matt.* **18** 4845 (2006).
2. D. Nuzhnyy, J. Petzelt, S. Kamba, P. Kužel, C. Kadlec, V. Bovtun, M. Kempa, J. Schubert, C. M. Brooks, and D. G. Schlom, *Appl. Phys. Lett.* **95**, 232902 (2009).
3. N. Sai and D. Vanderbilt, *Phys. Rev. B*, **62** 13942 (2000).
4. K. Uchida, S. Tsuneyuki, and T. Schimizu, *Phys. Rev. B* **68** 174107 (2003).
5. Y. Xie, *et al.*, *J. Phys.:Cond.Matt.*, **19** 5062123 (2007).
6. A. Ohtomo and H. Y. Hwang, *Nature (London)* **427**, 423 (2004).
7. W. Siemons, G. Koster, H. Yamamoto, W. A. Harrison, G. Lucovsky, T. H. Geballe, D. H. A. Blank, and M. R. Beasley, *Phys. Rev. Lett.* **98**, 196802 (2007).
8. A. Kalabukhov, R. Gunnarsson, J. Börjesson, E. Olsson, T. Claeson, and D. Winkler, *Phys. Rev. B* **75**, 121404 (2007).
9. S. Thiel, G. Hammerl, A. Schmehl, C. W. Schneider, and J. Mannhart, *Science* **313**, 1942 (2006).
10. N. Nakagawa, H. Y. Hwang, and D. A. Muller, *Nat. Mater.* **5**, 204 (2006).
11. A. S. Kalabukhov, Y. A. Boikov, I. T. Serenkov, V. I. Sakharov, V. N. Popok, R. Gunnarsson, J. Börjesson, N. Ljustina, E. Olsson, D. Winkler, et al., *Phys. Rev. Lett.* **103**, 146101 (2009).
12. S. S. A. Seo, M. J. Han, G. W. J. Hassink, W. S. Choi, S. J. Moon, J. S. Kim, T. Susaki, Y. S. Lee, J. Yu, C. Bernhard, H. Y. Hwang, G. Rijnders, D. H. A. Blank, B. Keimer, and T. W. Noh, *Phys. Rev. Lett.* **104**, 036401 (2010).

13. J. K. Lee and A. A. Demkov, Phys. Rev. B **78**, 193104 (2008).
14. J. Gordon, H. Shechter, and M. Folman, Phys. Rev. B **49** 4898 (1994).
15. B. Kierren and D. Paget, J. Vac. Sci. Technol. A **15**, 2074 (1997).
16. J. L. Larue *et al.*, J. Chem. Phys., **129** 024709 (2008).
17. A. W. Grant and C.T. Campbell, Phys. Rev. B, **55** 1844 (1997).
18. H. Hamamatsu *et al.*, Phys. Rev. B, **57** 11883 (1998).
19. C. C. Hwang *et al.*, J. Vac. Sci. Technol. A, **18** 1473 (2000).
20. W.B. Sherman *et al.*, Phys. Rev. B, **62** 4545 (2000).
21. C. Hogan *et al.*, Phys. Rev. B, **68** 205313 (2003) and Phys. Rev. B, **69** 125332 (2004).
22. O. E. Tereshchenko, V.L. Alperovich, and A.S. Terekhov, JETP Lett. **79** 131 (2004).
23. K. Kimoto, T. Tada, and T. Kanayama, Jpn. J. Appl. Phys. Lett. **46** L110 (2007).
24. G. Kresse and J. Hafner, Phys. Rev. B **47**, 558 (1993).
25. G. Kresse and J. Furthmuller, Phys. Rev. B **54**, 11169 (1996).
26. K. M. Song and A.K. Ray, Phys. Rev. B, **50** 14255 (1994).
27. S. Carlesi *et al.*, Phys. Rev. B, **59** 11716 (1999).
28. H.Y. Xiao *et al.*, J. Chem. Phys. **122** 174704 (2005).
29. S. L. Dudarev, G. A. Botton, S. Y. Savrasov, C. J. Humphreys and A. P. Sutton, Phys. Rev. B **57**, 1505 (1998).
30. C. Mitra, C. Lin, J. Robertson and A.A. Demkov, Phys. Rev. B **86**, 155105 (2012).

31. C. Lin, C. Mitra and A.A. Demkov, Phys. Rev. B **86**, 161102(R) (2012)
32. J. Padilla and D. Vanderbilt, Surf. Sci. **418** 64 (1998).
33. B. Meyer, J. Padilla, and D. Vanderbilt, Faraday Discussions 114: The Surface Science of Metal Oxides. 1999. Royal Society of Chemistry, London.
34. V. Heine, Phys. Rev. **138** A1689 (1965).
35. M. Mrovec, *et al.*, Phys. Rev. B, **79** 245121 (2009).
36. W. Monch, *et al.*, Phys. Rev. Lett. **58** 1260 (1987).
37. J. Tersoff, Phys. Rev. B, **30** 4874 (1984).
38. A. A. Demkov *et al.*, Phys. Rev. B, **71** 195306 (2005).
39. R. T. Tung, Phys. Rev. B, 2001. **64** 205310 (2001).
40. M. Schluter, Phys. Rev. B, 1978. **17** 5044 (1978).
41. X. Zhang *et al.*, Phys. Rev. B, 2003. **68** 125323 (2003).
42. J. Robertson and C.W. Chen, Appl. Phys. Lett., **74** 1168 (1999).
43. S. Zollner *et al.* J. Vac. Sci. Technol. B, **18** 2242 (2000).
44. E. Courtens, Phys. Rev. Lett., **29** 1380 (1972).
45. N. Sai and D. Vanderbilt, Phys. Rev. B, **62** 13942 (2000).
46. M. S. Dresselhaus, G. Dresselhaus, and A. Jorio, *Group Theory: Application to the Physics of Condensed Matter*, ed. Springer. 2008.

## FIGURE CAPTIONS

**Figure 1 (color online):** The  $(\text{Cs})_7/(\text{STO})_9/(\text{vacuum})/(\text{STO})_9/(\text{Cs})_7$  double slab separated by vacuum with two identical interfaces. (a) The slab with the “hollow site” interface geometry. Cs atoms are positioned on top of a hollow site surrounded by four in plane oxygen atoms (b) The slab with the “oxygen site” interface geometry. The Cs atom is placed on top of oxygen.

**Figure 2 (color online):** (a) Schematic of the energy band diagram of Cs and  $\text{TiO}_2$ -terminated STO before contact, (b) Schematic of the energy diagram of Cs and  $\text{TiO}_2$ -terminated STO in contact.

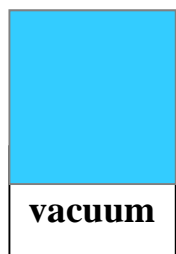
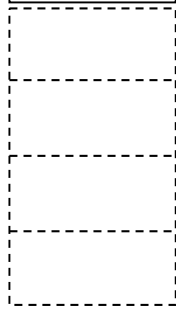
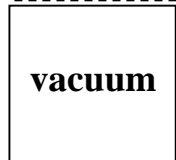
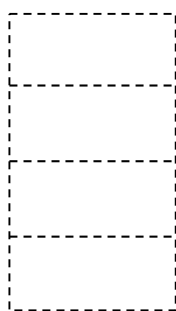
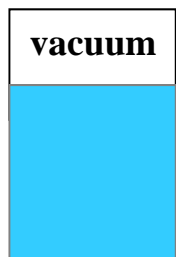
**Figure 3 (color online):** (a) FE-like atomic configuration of STO for the “hollow site” interface after the full lattice relaxation of the Cs/STO slab. Rumpling for each  $\text{TiO}_2$  layer along the stacking direction. (b) AFD distortions of STO for the “oxygen site” interface after lattice relaxation of Cs/STO. Rotation of the octahedra for each  $\text{TiO}_2$  layer along the stacking direction.

**Figure 4 (color online):** (a) The projected density of states of two Cs/STO slabs with different interface geometries along the stacking direction. Zero is set at the Fermi level. In both cases, charge transfer is complete within two layers of STO. The electronic structure is recovered to that of bulk STO (thick red arrow) by the 3<sup>rd</sup>  $\text{TiO}_2$  layer. The surface oxygen state is 0.9 eV ( $\Delta$ s) higher than the bulk valence band top. (b) The number of electrons penetrating into gap states for CS/STO slabs with two different interface geometries (note the log scale)

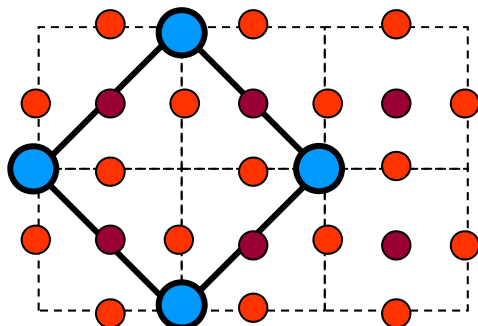
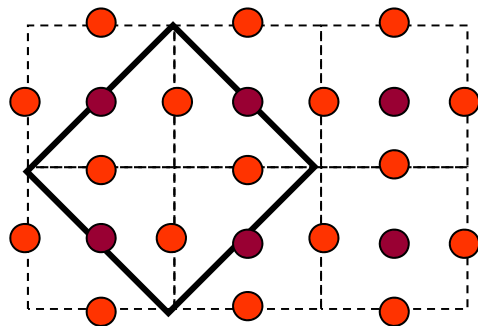
**Figure 5 (color online):** (a) Octahedral and square pyramidal crystal field diagram for Ti atom including the 4p contribution. Under the square pyramidal crystal field, the hybridization between Ti  $4p_z$  and  $3d_z^2$  pushes  $3d_z^2$  level down in energy, leading to an

orbital order [44]. (b) Orbital decomposed DOS of an interfacial Ti atom for the Cs/STO slab with the AFD distortion. The Ti  $3d_z^2$  is 1.5 eV below  $3d_x^2-y^2$  due mainly to a strong hybridization with Ti  $4p_z$  components.

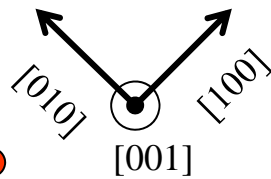
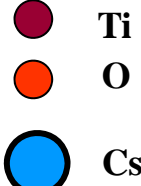
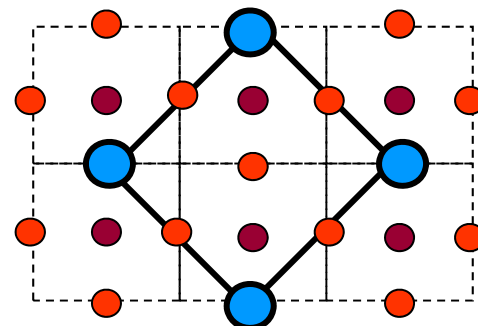
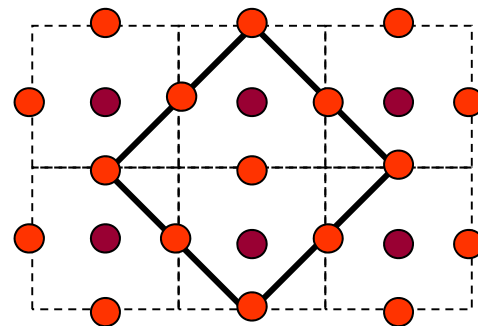
**Figure 6 (color online):** The isosurface plot of transferred charge distribution for the Cs/STO slab with the AFD distortion (a) and FE-like distortion (b). In both cases, the interfacial charge distributions inside STO are dumbbell-like, indicating the  $3d_z^2$  orbital order.

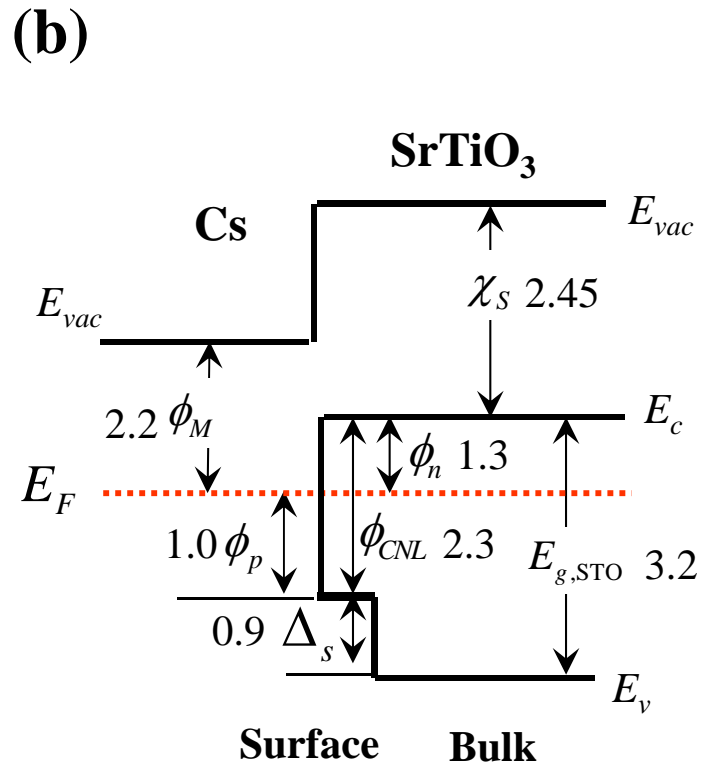
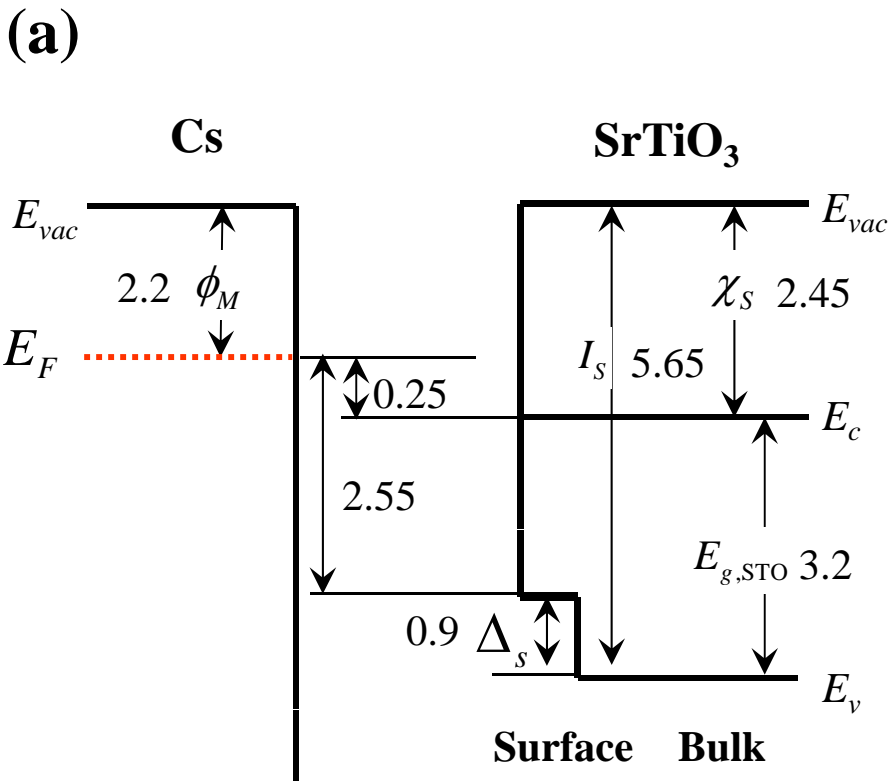


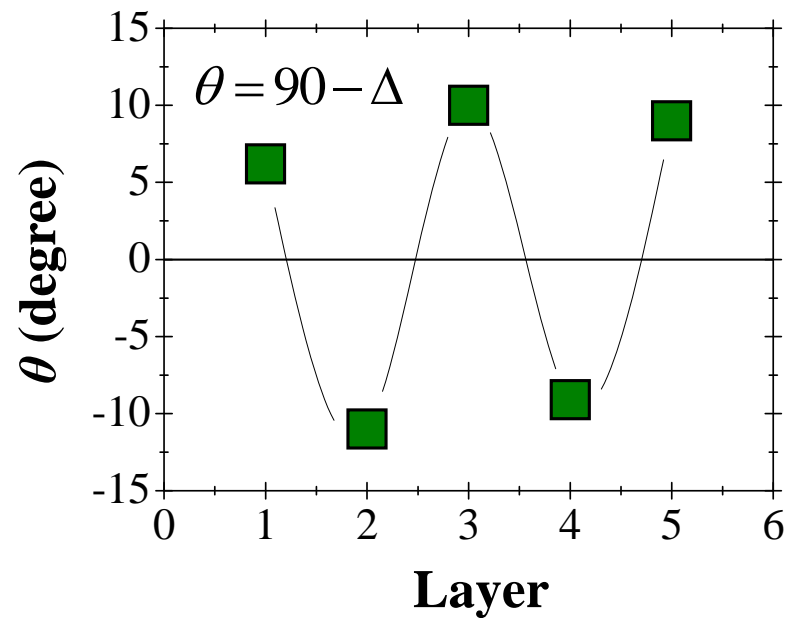
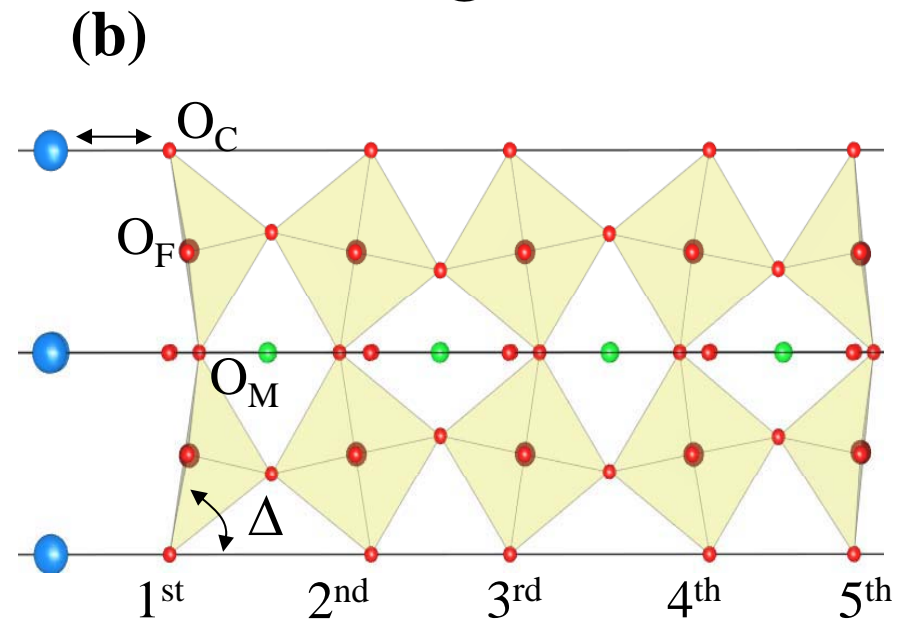
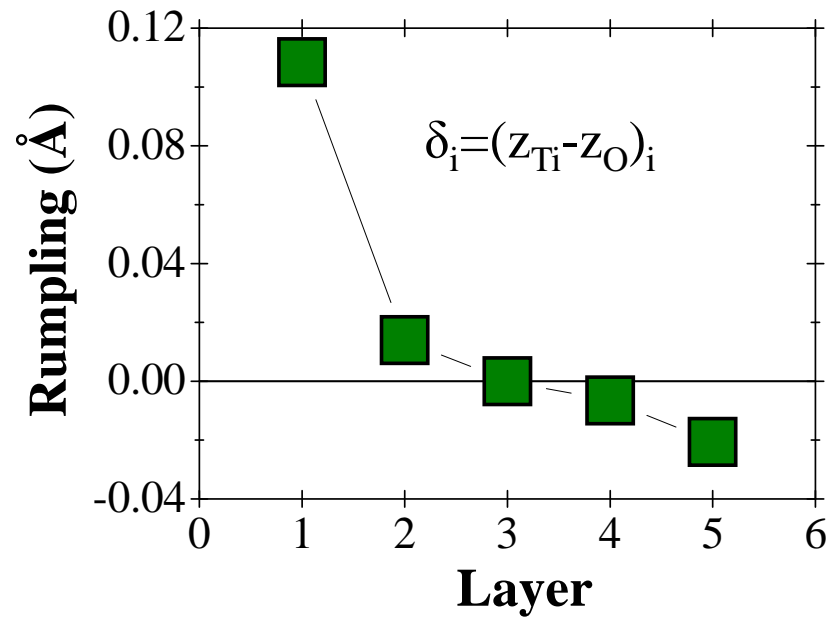
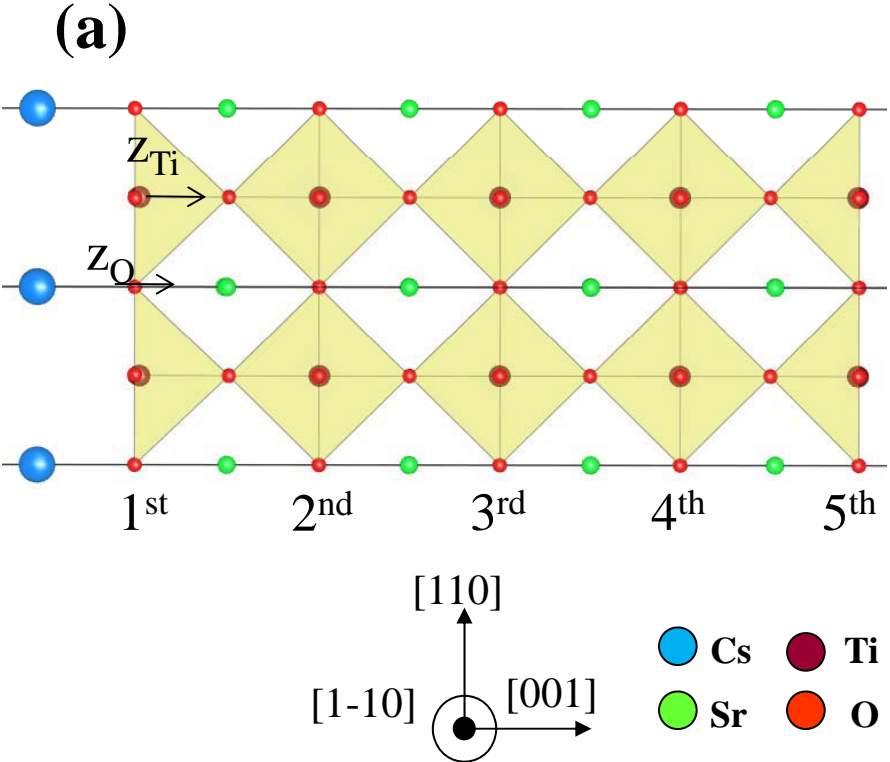
**(a)**

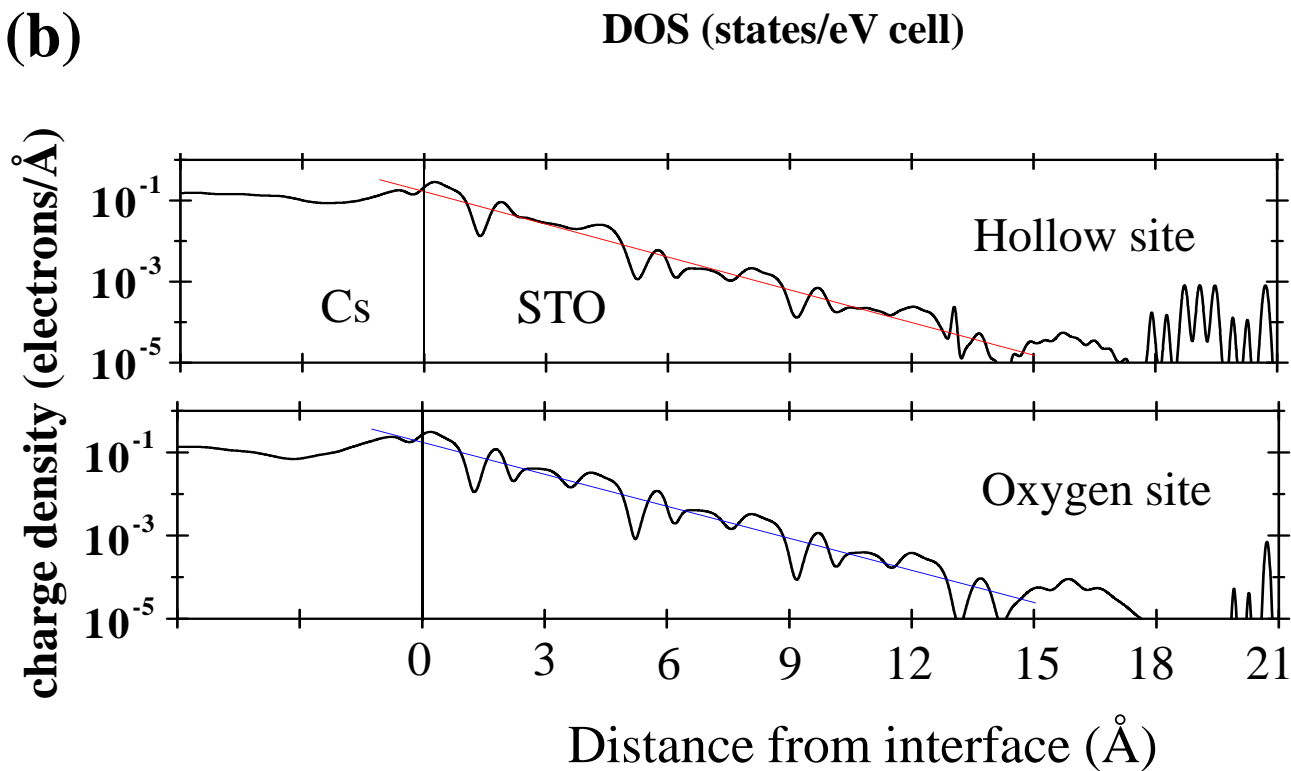
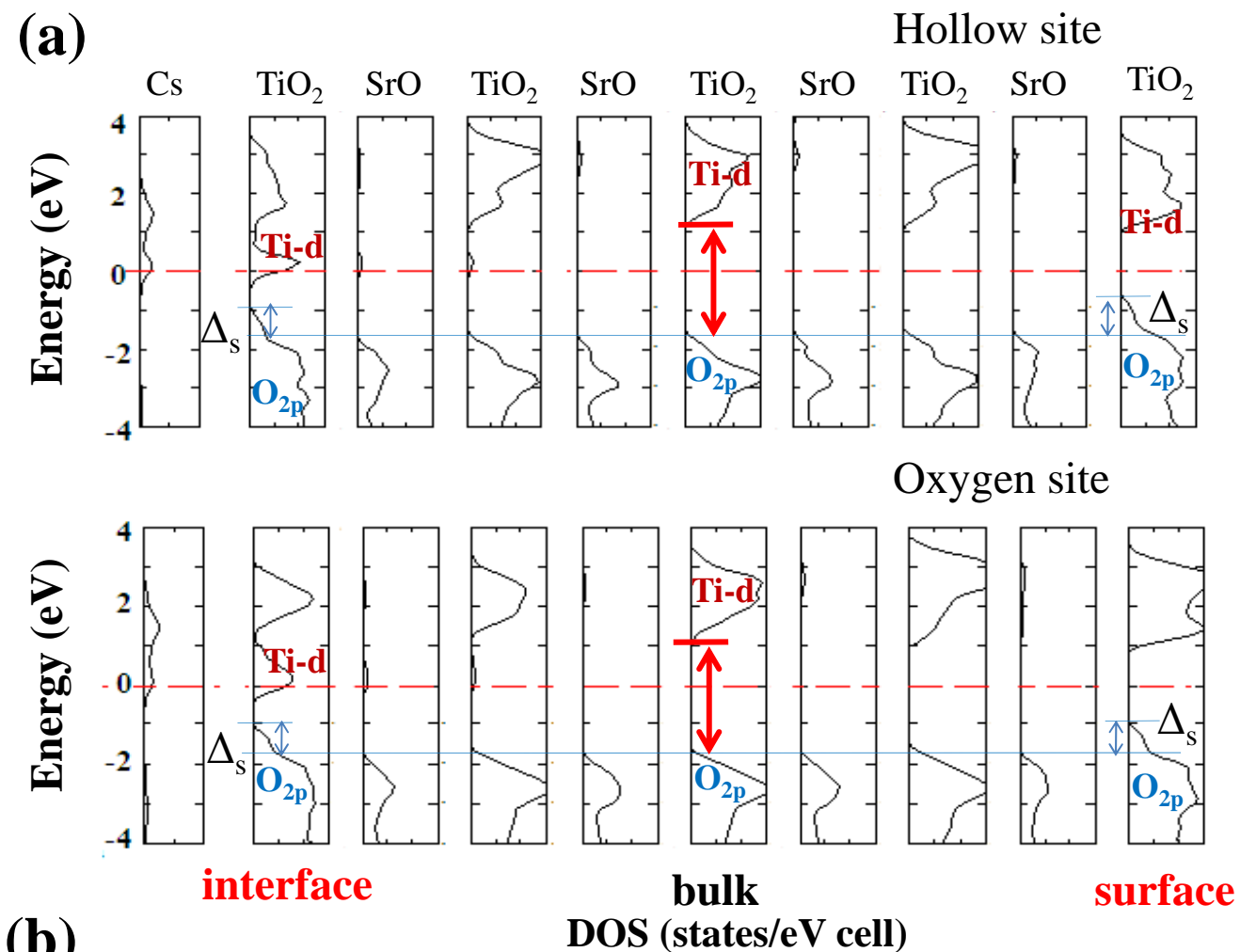


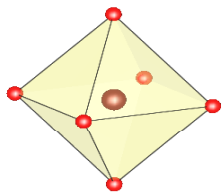
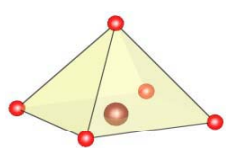
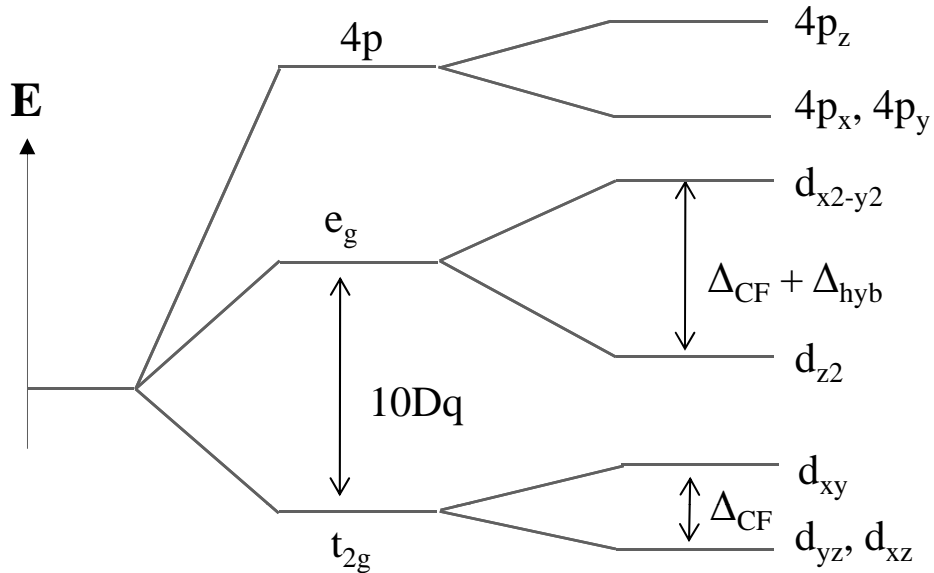
**(b)**









**(a)**Octahedral  
symmetrySquare pyramidal  
symmetry**(b)**